

© 2008 IEEE

Mechronic and Embedded Systems and Applications, 2008. MESA 2008

## Design Considerations and Experimental Results of a 60 W Compressed-Air-to-Electric-Power System

<b>Daniel Krähenbühl</b>	ETH Zürich, Switzerland
<b>Christof Zwysig</b>	ETH Zürich, Switzerland
<b>Hansulrich Hörler</b>	ETH Zürich, Switzerland
<b>Johann W. Kolar</b>	ETH Zürich, Switzerland

This material is posted here with permission of the IEEE. Such permission of the IEEE does not in any way imply IEEE endorsement of any of Celeroton's products or services. Internal or personal use of this material is permitted. However, [no recopying, reprinting, redistributing or reselling is permitted without the written consent from IEEE](#). By choosing to view this document, you agree to all provisions of the copyright laws protecting it.

# Design Considerations and Experimental Results of a 60 W Compressed-Air-to-Electric-Power System

D. Krähenbühl<sup>1</sup>, C Zwysig<sup>1</sup>, H. Hörler<sup>2</sup> and J. W. Kolar<sup>1</sup>

<sup>1</sup>Power Electronic Systems Laboratory, ETH Zurich, Switzerland

<sup>2</sup>Aerothermochemistry and Combustion Systems Laboratory, ETH Zurich, Switzerland

**Abstract**—In many process applications, where a pressure reduction is required the energy ends up being dissipated as heat. Examples are throttling valves of gas pipelines and automotive engines or turbo expanders as used in cryogenic plants. With a new pressure reduction system that produces electricity while expanding the gas, this lost energy can be recovered. To achieve a high power density this energy generation system requires an increased operating speed of the electrical machine and the turbomachinery. This paper proposes a miniature compressed-air-to-electric-power system, based on a single-stage axial impulse turbine with a rated rotational speed of 350 000 rpm and a rated electric power output of 60 W. A comprehensive description including turbine and permanent magnet (PM) generator is given and measurements like maximum electric output power of 124 W and maximum system efficiency of 24 % are presented.

## I. INTRODUCTION

In pressure reduction devices, such as valves, conventional throttles or turbo expanders, the excess process energy is usually wasted as heat. However, this energy could be recovered by employing a system that removes the energy from pressurized gas flow and converts it into electrical energy.

One example is the replacement of the conventional throttle in automotive applications where a turbine in combination with a generator can actively throttle the intake air and thereby produce electrical power [1]. Measurements at constant speed have shown that up to 700 W electric power could be produced (turbine  $\varnothing$  40 mm) and an extrapolation with a 50 % downsized turbine predicts that even more electric power could be produced.

While it is necessary to transport natural gas at high pressures, end-users require gas delivery at only a fraction of the main pipeline pressure. Therefore, energy can be recovered at pressure reduction stations if throttling valves are replaced by expanders driving electrical generators [2]. For power recovery, turbines are generally rated from 150 kW to 2.5 MW, however, the pressure reduction process is usually done in several stages, and an array of small turbine-generator modules could replace one large pressure reduction valve [3]. Also, the turbo expanders used today in cryogenic plants transfer the excess power (in the kW range) to a brake compressor where the energy is finally dissipated into cooling water. If a generator would be employed for the braking of the turbo expander, energy could be recovered, and therefore the efficiency of such plants could be increased [4].

Several of the abovementioned applications, e.g. in automobiles, need ultra-compact power generation systems.

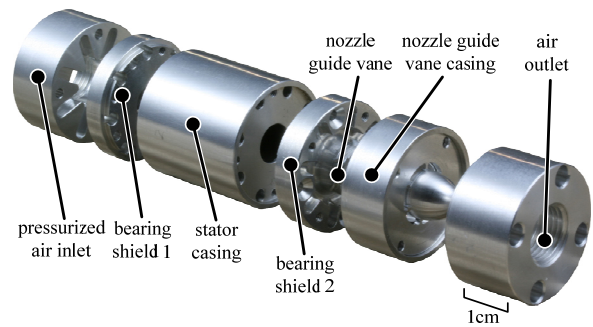


Fig. 1. Picture of the ultra compact (22 mm x 60 mm) air-to-power demonstrator.

Power density in both turbomachinery and electrical machines increases with increasing rotational speed [5], [6]. Therefore, for highest power density, these systems are operating at speeds between 100 000 rpm and 1 Mrpm at power levels of up to several kilowatts. Besides higher power applications, micro-turbines with less than 100 W power output and very high speeds have been reported in literature. In [7], a modular system consisting of an off-the-shelf air turbine from a dental drill, a permanent-magnet (PM) generator and a rectifier has been realized, with a maximal power output of 1.11 W and a maximal speed of 200 000 rpm. Drawbacks of this system are the poor power density ( $0.02 \text{ W/cm}^3$ ) and the large inlet flow rate of 45 l/min at maximum power output. The power electronics of the system consists of a three-phase transformer a diode bridge rectifier and a 5 V linear regulator.

In [8], a single-stage axial micro gas turbine coupled to a commercial electrical machine with a maximal electric power output of 16 W at 160 000 rpm and 1 bar supply pressure has been introduced for later use in a gas turbine system. The maximal torque and mechanical power generated from the turbine is 3.7 mNm, respectively 28 W. The generator is connected to a variable three phase resistive load to measure the electric output power. The total system has a maximum efficiency of 10.5 % at 100 000 rpm and achieves a power density of  $1.6 \text{ W/cm}^3$ , excluding power and control electronics.

In [9], a PM generator, capable of supplying 8 W of dc power to a resistive load at a rotational speed of 305 000 rpm is shown. The stator uses interleaved, electroplated copper windings on a magnetically soft substrate. The rotor consists of an 8-pole SmCo PM, back iron and a titanium sleeve, because of the high centrifugal forces. The machine was characterized using an air-driven spindle. To provide a dc voltage, the ac generator voltages were first stepped up using a three-phase transformer and then converted to dc using a

three-phase Schottky diode bridge rectifier. The dimensions of the device are chosen with reference to a future integration into a micro turbine engine. This leads to a generator power density of  $59 \text{ W/cm}^3$  and to a generator efficiency of 28 %.

A planar generator with a diameter of 8 mm consisting of a permanent magnet disc rotor cut out of bulk SmCo or NdFeB protected by a titanium sleeve, and a silicon stator with electroplated three-phase planar coils is presented in [10]. The generator is driven by a planar turbine, etched in the other side of the rotor. Due to the turbine construction, the speed is limited to 100 000 rpm with 5 bar compressed air supply. A maximum power output of 14.6 mW was measured at 58 000 rpm with three Y-connected  $50 \Omega$  resistors. Using a turbine of a dental drill, the rotor reached a maximum speed of 420 000 rpm. With this setup, the highest electric power output of 5 W (three Y-connected  $12 \Omega$  resistors) was reached at 380 000 rpm with an electric efficiency of 66 %.

In [11], a compressed-air-to-electric-power system with a rotational speed of 490 000 rpm and a power output of 150 W is presented. The system is based on the reversal of an existing turbocompressor system which reaches a maximal pressure ratio of 1.6 at a maximal rotational speed of 550 000 rpm and an electric power input of 150 W. It is driven by a low voltage power electronics with 28 V dc input. With new and specially designed nozzle guide vanes, the turbo compressor system can be reversed and operated as a turbine system.

In this paper, a compressed-air-to-electric-power system with a rated rotational speed of 350 000 rpm and a rated power output of 60 W is presented (Fig. 1). First, different turbines are described and compared, and then a full description of the system is given. This compressed-air-to-electric-power system comprises of a single-stage axial impulse turbine (Laval turbine), a PM-generator and the power and control electronics. Secondly, measurements like mass flow, electric output power and efficiencies of the different system parts are presented.

## II. TURBINE SELECTION

There are several options for the turbine which are compared concerning, e.g., size, efficiency, rotational speed, and simplicity in manufacturing.

### A. Axial Turbine

#### 1) Single-stage axial impulse turbine (Laval turbine)

In impulse turbines, the drop in pressure (expansion) of pressurized air takes place only in the stationary nozzles and not between the moving rotor blades ( $p_2 \approx p_3$ ). This is obtained by making the blade passage of constant cross-sectional area. The nozzle vanes produce a jet of air of high velocity and the blades change the direction of the jet, thus producing a change in momentum and a force that propels the blades. Advantages of an impulse turbine are the small leakage losses because of the small pressure gradient over the rotor blades, lower rotating speed compared with the reaction turbine and a minimal axial thrust which results in low friction losses in the bearings. A further advantage of this turbine type is the simple construction and the possibility to use a shrouding band,

which would lead to a higher efficiency. Disadvantages of an axial turbine are the losses in the nozzles because of the high acceleration of the pressurized air, and the blade losses because the air is highly deflected. These main disadvantages lead to lower efficiencies than for reaction and radial turbines.

#### 2) Single-stage axial reaction turbine

In reaction turbines a part of the expansion of compressed air takes place between the rotor blades. For a reaction of 0.5 the expansion takes place in equal shares in the stationary nozzles and between the rotor blades. Drawbacks of a reaction turbine are the additional friction losses in the bearings, because of additional axial thrust, due to the pressure gradient over the rotor blades and the more complex construction. Advantages are the better efficiency and also the possibility of adding a shrouding band.

### B. Radial Turbine

#### Inward-flow radial (IFR) turbine

Concerning the efficiency the radial turbine is the best choice, but there are some major disadvantages: For low flow rates the blade height of the turbine ( $< 0.5 \text{ mm}$ ) or the turbine diameter get very small ( $< 1 \text{ cm}$ ). This leads to expensive turbines which are difficult to manufacture. Also the curved geometry of the rotor blades, the spiral casing and the radial outlet lead to a difficult production. Due to the higher rotating speed the life time of the bearing is reduced.

### C. Further Systems

#### Reciprocating engine

Theoretically, a reciprocating engine could be used instead of an axial- or radial turbine. However the disadvantages like the piston lining, lubrication and vibrations and the rather low speed (e.g. big size of the generator) are so dominant that this approach is not an option.

Due to simplicity, size and rotating speed a single-stage axial impulse turbine has been chosen.

## III. TURBINE AND NOZZLE GUIDE VANE DESIGN

### A. Turbine Design

Assuming adiabatic flow through the turbine, the corresponding ideal enthalpy temperature drop  $\Delta T_{(1-3s)}$  can be calculated with

$$\Delta T_{(1-3s)} = T_1 \left( 1 - \frac{p_1}{p_3} \left( \frac{1}{\kappa} \right)^{\kappa-1} \right) = 80.8 \text{ K} \quad (1)$$

$$T_{3s} = T_1 - \Delta T_{(1-3s)} = 219.2 \text{ K} \quad (2)$$

with  $p_1 = 3 \text{ bar}$ ,  $p_3 = 1 \text{ bar}$  and  $T_1 = 300 \text{ K}$ . For the real expansion the increase of entropy, e.g. losses, must be considered. The isentropic efficiency  $\eta_{is}$  was assumed to be 30 %, which leads to the actual expansion drop of

$$\Delta T_{(1-3)} = \Delta T_{(1-3s)} \eta_{is} = 24.2 \text{ K} \rightarrow T_3 = 275.8 \text{ K} \quad (3)$$

and to the theoretical mass flow of

$$\dot{m} = \frac{P_{mech}}{c_p \Delta T_{(1-3s)} \eta_{is}} = 2.5 \frac{\text{g}}{\text{s}} \quad (4)$$

where  $c_p$  is the specific heat capacity and  $P_{mech} = 60 \text{ W}$ . The

effective turbine inlet area  $A$  (and thereby the radii  $r_1$ ,  $r_2$  and  $r_3$ ) can be calculated with the flow function, described in [12]. Furthermore, the velocity diagram at rotor entry and rotor outlet can be calculated as shown in Fig. 2. The relatively large absolute velocity  $c_2 = 335$  m/s is near the sonic speed.

### B. Nozzle Guide Vanes Design

Due to the fact that the selected turbine type is an impulse turbine, the pressure drop, e.g. the acceleration of the air, fully takes place in the nozzle guide vanes. This means that the outer inlet area decreases, e.g. the radius  $r_1$  reduces to  $r_2$ , while  $r_3$  remains constant, and the nozzle guide vane output area equals the turbine inlet area. The second important function of the guide vanes is the deflection of the air stream to the correct angle, such that the velocity diagram is consistent as shown in Fig. 2.

### C. Leakage Losses

All turbomachines suffer from losses associated with the leakage of some fluid around rotors and stators. Tip leakage is driven by the pressure difference between the blade suction and pressure side. Also the manufacturing tolerances cannot be decreased proportional with the turbine scaling, therefore the leakage losses become more dominant for small turbines. Due to the fact that the rotor blades are only 0.5 mm high, the tip clearance between rotor and casing must be as low as possible. The first measurement was made with a tip clearance of 0.1 mm ( $d_c/d_h = 20\%$ ), which is clearly too much. For big turbomachinery the tip clearance is in the range of 1% to 2% of the rotor height. Therefore, for the further measurements tip clearance must be reduced to values below 10%.

### D. Reynolds Number

The Reynolds number characterizes the flow in the turbine (laminar / turbulent) and is defined as

$$\text{Re} = \frac{cd_h}{\nu} \quad (5)$$

where  $c$  denominates the speed of the airflow,  $d_h$  the height of the air flow channel (rotor height) and  $\nu$  the kinematic viscosity. As a consequence of miniaturization, the Reynolds number will decrease, and therefore the flow will become more laminar. In the used axial turbine the Reynolds number is in the range of 11 000, with is still in the area of turbulent air flow.

## IV. ELECTRICAL CONSIDERATIONS

The rotor of the PM generator consists of a diametrically magnetized cylindrical SmCo or NdFeB permanent magnet encased in a retaining titanium sleeve ensuring sufficiently low mechanical stresses on the magnet. The eccentricity is minimized by shrink fitting the sleeve on the permanent magnet and grinding the rotor. Additionally, the fully assembled rotor is balanced.

The stator magnetic field rotates with high frequency (5.8 kHz), it is therefore necessary to minimize the losses in the stator core by using amorphous iron. In order to minimize the eddy current losses in the three-phase air-gap copper winding, the winding is realized with litz-wire. The motor has

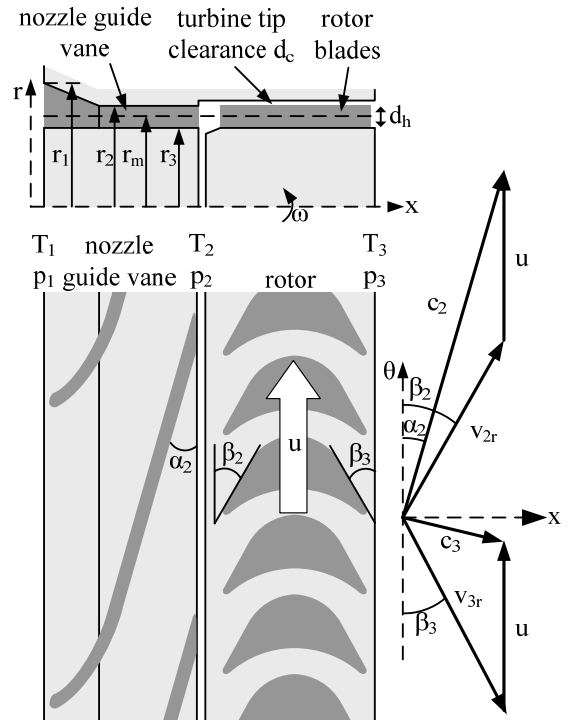


Fig. 2. Drawing of the single-stage axial impulse turbine (Laval turbine) with  $r_m = 4.5$  mm and the corresponding nozzle guide vane and velocity diagrams at rotor inlet and outlet for the rated rotational speed.  $c_2$  and  $c_3$  are the absolute velocities at the rotor inlet and outlet.  $v_{2r}$  and  $v_{3r}$  are the relative velocities at the rotor inlet and outlet.  $u$  is the rotor speed at radius  $r_m$ .

TABLE I: COMPUTED THERMODYNAMIC DATA

Parameter	Description	Value	Unit
$T_1$	Inlet air temperature	300	K
$p_1$	inlet pressure	3 - 8	bar
$p_3$	outlet pressure	1	bar
$\eta_n$	nozzle guide vane efficiency	90	%
$\eta_{is}$	isentropic efficiency	40	%
$r_m$	median radius	4.5	mm
$d_h$	rotor blade height	0.5	mm
$n_r$	rated speed	350 000	rpm
$u$	rated stator speed at $r_m$	165	m/s

TABLE II: MEASURED GENERATOR DATA

Parameter	Description	Value	Unit
$n_{max}$	maximum speed	500 000	rpm
$\Psi_{PM}$	magnet flux linkage	0.32	mVs
$U_{ind}$	back EMF at rated speed	11.7	V
$L_S$	stator inductance	2.1	$\mu$ H
$R_S$	stator resistance	0.12	$\Omega$

a peak phase-to-phase voltage of 20.2 V at 350 000 rpm (with the NdFeB permanent magnet). The generator design has been optimized, considering the total losses [13] (not included in the optimisation process are the bearing losses), therefore, in the rated operating point of the turbine the generator efficiency is 93%. A detailed description of a similar motor/generator has been presented in [14]. In Table II the measured electrical data of the PM generator is summarized, and in Fig. 3 the computed efficiency of the generator in the entire power-speed plane is shown.

The first measurements were made with varying a resistive three-phase load. In a second step, a bi-directional power electronics consisting of an active three-phase rectifier and an additional boost converter will be used. The power electronics, analyzed in [15], shows an efficiency of 95% at rated power.

The output of the system is controlled to 24 V dc, allowing for direct connection to applications/loads in contrary to the variable dc output voltage in [7] and the variable three-phase ac voltages in [8].

## V. SYSTEM INTEGRATION

In Fig. 4 a solid model of the compressed-air-to-electric-power system is shown. In the following section the system integration, e.g. the air flow, the rotor dynamics and the power density is described.

### A. Air Flow

The compressed air enters through a common pneumatic connector that can be screwed into the system on the right hand side. The pressurized air then gets diverted into eight channels that are arranged symmetrically in the generator casing and the ball bearing shields (indicated with arrows in Fig. 4). This leads to higher effort in the construction of the casing, but the generator and the ball bearings can be cooled and as a positive side effect, the inlet air gets heated up which leads to higher outlet air temperature and therefore less problems with dew point and icing. Calculations show that the temperature rise due to waste heat from the generator is in the range of 5 K. The pressurized inlet air then reaches the nozzle guide vanes. In the first part of the nozzle guide vanes the area is decreased to the effective turbine area and thereby the pressurized air is accelerated and the pressure drops to almost outlet pressure. In the second part the accelerated air is diverged to the right angle  $\alpha_2$ . The air then passes through the turbine and leaves the system on the left hand side to the environment. A detailed view of the air flow in the nozzle guide vanes and the turbine can be seen in Fig. 1 and Fig. 2.

### B. Rotor Dynamics

In order to run the system in between two critical speeds, the bending modes of the rotor and turbine assembly are determined with finite element simulations. The spring constant of the bearing system is taken into account, which shifts the bending modes to lower frequencies. The length of the shaft is adjusted such that rated speed (350 000 rpm, 5833 Hz) falls between the second (285 420 rpm) and the third (723 900 rpm) bending mode (Fig. 5). In Fig. 6 a picture of the axial impulse turbine and rotor with assembled high speed bearings is shown.

### C. Power Density

The integrated system has a volume of  $22.8 \text{ cm}^3$  ( $d = 2.2 \text{ cm}$ ,  $l = 6 \text{ cm}$ ) and the electronics interface has a volume of  $60.8 \text{ cm}^3$  ( $l = 4.5 \text{ cm}$ ,  $b = 4.5 \text{ cm}$ ,  $h = 3 \text{ cm}$ ). This leads to a maximal generator and turbine power density of  $4.4 \text{ W/cm}^3$  and of  $0.8 \text{ W/cm}^3$  including the power and control electronics. Due to the fact that the electronics were made for motor applications and not for compact generator applications, a specific redesign and integration will increase the overall power density of the system. Integrating the power electronics into the turbine-generator system will avoid an additional heat sink if it is thermally attached to the generator casing and thereby cooled by the air flow.

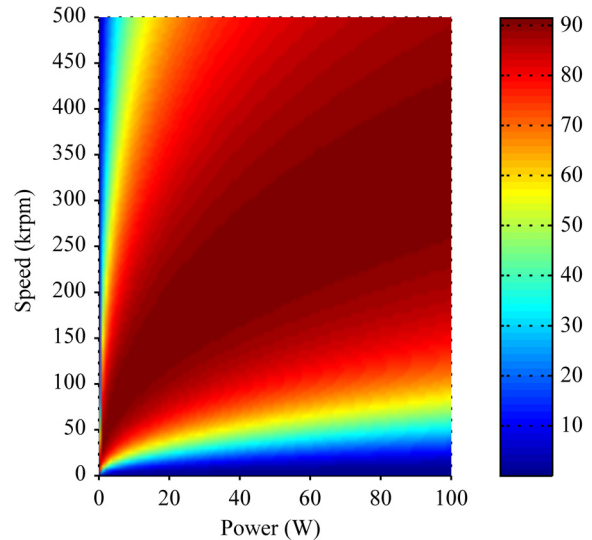


Fig. 3. Computed efficiency of the generator (including bearing losses).

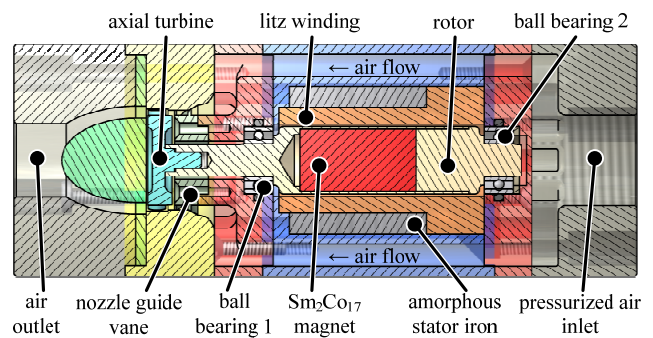


Fig. 4. Solid model of the ultra compact (22 mm x 60 mm) air-to-power demonstrator.

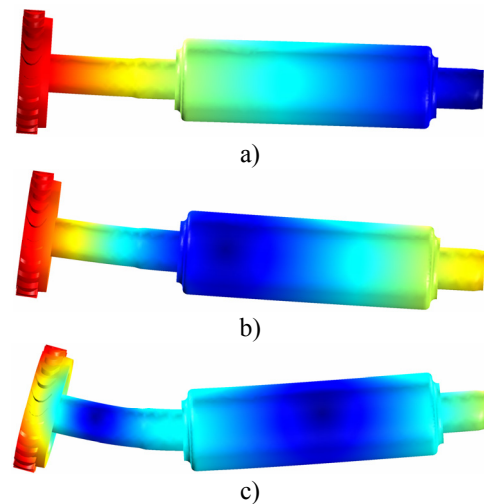


Fig. 5. Bending modes of the rotor. First bending mode at 198 840 rpm, 3314 Hz (a), second bending mode at 285 420 rpm, 4757 Hz (b) and third bending mode at 723 900 rpm, 12065 Hz (c).

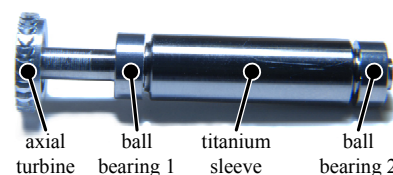


Fig. 6. Impulse turbine and rotor with assembled high speed bearings.

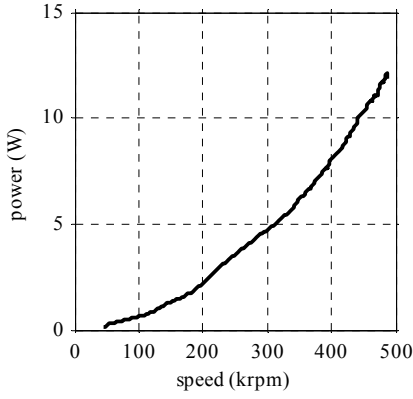


Fig. 7. Measured losses of the high speed motor over speed. The total power losses include the bearing losses, windage losses and core losses.

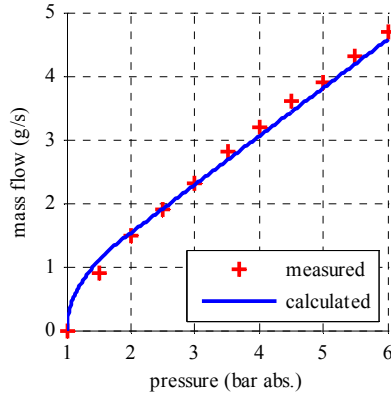


Fig. 8. Measured and calculated mass flow as a function of the inlet pressure.

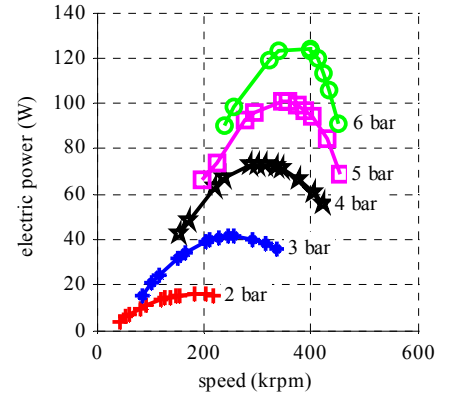


Fig. 9. Electrical power generated by the turbine and generator system as a function of speed and supply pressure.

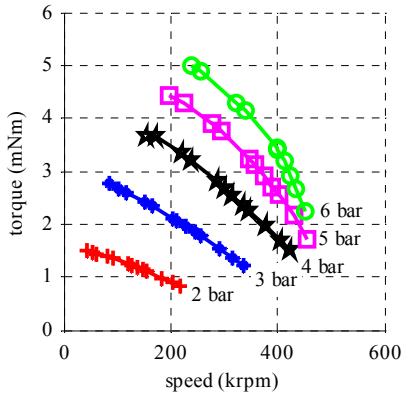


Fig. 10. Torque generated by the turbine as a function of speed and supply pressure.

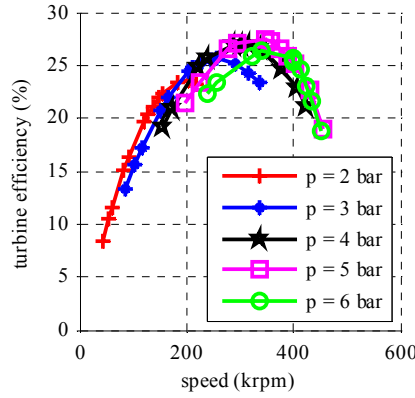


Fig. 11. Turbine efficiency as a function of speed and inlet pressure.

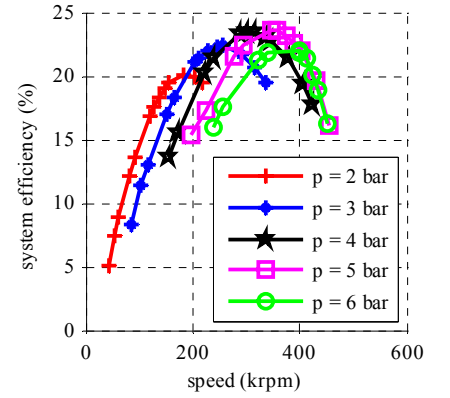


Fig. 12. System efficiency as a function of speed and inlet pressure.

## VI. MEASUREMENTS

An experimental test bench is built in order to verify theoretical considerations and the compressed-air-to-power system concept. It includes a mass flow sensor and several thermocouples and pressure sensors and the three-phase variable resistive load. Measurements of mass flow, electric output power and efficiencies of the different system parts will be presented in the following. The system has been tested up to an inlet pressure of 6 bar and a maximal outlet electric power of 124 W. The turbine-generator-system has been built with a rotor tip clearance of 0.1 mm and without a shrouding band.

### A. Measurement Setup

For the measurement, the operating point could be changed by varying the resistive three-phase load and the supply pressure. Additionally to input and output pressure, the input and output temperature of the air flow has been measured. As expected, the efficiency could not be calculated depending on the temperature drop, because the turbine is not sufficiently isolated from the thermal losses of generator and the ball bearings. At the first possible temperature measurement point after the turbine the air is already heated up. For better verification the mass flow has been measured in the low and

high pressure side. The pressurized air to electric power efficiency has been calculated using

$$\eta_{air,el} = \frac{P_{el}}{\dot{m} \cdot \Delta T_{(1-3s)} \cdot c_p} \quad (6)$$

with  $\Delta T_{(1-3s)}$  from (1). The isentropic efficiency of the axial turbine can now be calculated with the measured efficiency of the generator shown in Fig. 7 (the copper losses must be added separately, described in VI.B).

### B. Initial Measurements

Since the rotor bending modes, and the interference fit of rotor sleeve and the permanent magnet have been designed for a maximal speed of 500 000 rpm, the generator could first be tested as a motor up to a speed of 500 000 rpm. Thereby, the losses at the rated speed of 350 000 rpm (6.2 W) and at 500 000 rpm (13 W) were measured (Fig. 7). For measuring the bearing, windage and core losses a deceleration test was used. This method is based on the fact that in open loop operation (no electrical drive or break) the rotational energy is used up by the losses, decreasing the rotational speed accordingly. The gradient of this deceleration is a measure for the losses. The dynamical equation for the rotor is

$$J \frac{d\omega}{dt} = -T_{Loss} = -\frac{P_{Loss}}{\omega} \quad (7)$$

where  $\omega$  is the angular frequency,  $J$  the calculated rotor inertia ( $2 \cdot 10^{-8} \text{ kgm}^2$ ),  $T_{Loss}$  the total friction torque and  $P_{Loss}$  the total losses. Not included in the deceleration test are the copper losses depending on the phase currents. The copper losses can easily be added if the phase currents are measured during generator operation.

### C. Mass flow Measurements

In Fig. 8 the measured and calculated mass flow through the turbine is plotted. It can be seen, that the measured mass flow can be very well calculated with the flow function described in [12]. Also, the predicted dependence of mass flow (and therefore input power) and supply pressure in (4) can be verified; the mass flow does not depend on speed or load. A maximal mass flow of 4.7 g/s at 6 bar inlet pressure was achieved.

### D. Speed Measurements

Fig. 9 and Fig. 10 show the electric output power and torque as a function of speed and supply pressure. The maximal electric power output is around 124 W at 370 000 rpm and the maximal measured torque is 5 mNm at 240 000 rpm.

An increase of the resistive load causes a decrease of the torque and therefore an increasing speed at a constant supply pressure. The turbine generator system has been tested up to 455 000 rpm and 6 bar supply pressure.

### E. Efficiency Measurements

Fig. 11 and Fig. 12 show the turbine and the system efficiency as a function of speed and supply pressure. The maximum turbine efficiency is about 28 %, while the maximum system efficiency is 24 %. This can be compared to [8], where the system efficiency is 10.5 %. The maximum turbine efficiency is not as high as assumed in III.A. This is mainly due to the large tip clearance and the absence of a shrouding band.

## VII. CONCLUSION

This paper shows the design and measurement results of a compressed-air-to-electric power system. The described system has been optimized concerning power density ( $4.4 \text{ W/cm}^3$ ) and system efficiency ( $\eta_{System} = 24 \%$ ); the computed and measured values are significantly higher compared to similar systems described in literature so far. Also the generator efficiency (87 %) is significantly higher compared to [8] (58 %) and [9] (28 %), respectively. The better efficiencies can be achieved by system integration, generator optimization and careful design of the turbine. Due to the miniaturization, the isentropic efficiency cannot be predicted analytically and has been verified experimentally.

Measurements show that the system has a maximum power output of 124 W at 370 000 rpm and a maximum efficiency of 24 % at 350 000 rpm.

In a next step the tip clearance will be further reduced and the use of a shrouding band will be investigated. Future steps are the integration of the power electronics and a valve into the system and the implementation of a digital control in order to provide a constant dc output voltage for variable loads.

## REFERENCES

- [1] L. Guzzella, M. Betschart, T. Fluri, R. De Santis, C. Onder, T. Auckenthaler. *Recuperative Throttling of SI Engines for Improved Fuel Economy*. SAE 2004 World Congress & Exhibition, March 2004, Detroit, MI, USA.
- [2] A. Mirandola and L. Minca. *Energy Recovery by Expansion of High Pressure Natural Gas*. Proc. of the 21st Intersociety Energy Conversion Engineering Conference, Vol. 1, pp. 16-21, San Diego, California, Aug. 25-29, 1986.
- [3] B. Lehman and E. Worrell. *Electricity Production from Natural Gas Pressure Recovery Using Expansion Turbines*. Proc. 2001 ACEEE Summer Study on Energy Efficiency in Industry, Vol. 2, Tarrytown, NY, July 24-27th, 2001, pp. 43-54.
- [4] P. R. LeGoy. *Utility Requirements for Power Recovery in the Cryogenic and Chemical Industry Using Variable Frequency Drives in the Regenerative Mode*. The 1999 IEEE Power Engineering Society Summer Meeting, July 1999, Edmonton Alberta Canada.
- [5] A. Binder, T. Schneider. *High-Speed Inverter-Fed AC Drives*. International Aegean Conference on Electrical Machines and Power Electronics, Electromotion 2007, Bodrum, Turkey, Sept. 10-12, 2007.
- [6] S. Kang, S.-J.J. Lee, F.B. Prinz. *Size does matter, the pros and cons of miniaturization*. ABB Rev. 2 (2001) 54–62.
- [7] D.P. Arnold, P. Galle, F. Herrault, S. Das, J.H. Lang, and M.G. Allen. *A Self-Contained, Flow-Powered Microgenerator System*. Proceedings of the 5th International Workshop on Micro and Nanotechnology for Power Generation and Energy Conversion Applications (PowerMEMS 2005), Tokyo, Japan, Nov. 28 - 30.
- [8] J. Peirs, D. Reynaerts, F. Verplaetsen. *A Microturbine for Electric Power Generation*. Sensors and Actuators A: Physical Volume 113, Issue 1, 15 June 2004, pp. 86-93.
- [9] D. P. Arnold, F. Herrault, I. Zana, P. Galle, J.-W. Park, S. Das, J. H. Lang, and M. G. Allen. *Design optimization of an 8-Watt, microscale, axial-flux, permanent-magnet generator*. J. Micromech. Microeng., vol. 16, no. 9, pp. S290–S296, Sep. 2006.
- [10] H. Raisigel, O. Cugat, and J. Delamare. *Permanent magnet planar micro-generators*. Sensors and Actuators A: Volume 130–131, pp. 438–444, August 2006.
- [11] D. Krähenbühl, C. Zwyssig, H. Weser and J. W. Kolar. *Mesoscale electric power generation from pressurized gas flow*. Proceedings of the 7th International Workshop on Micro and Nanotechnology for Power Generation and Energy Conversion Applications (PowerMEMS 2007), Freiburg, Deutschland, Nov. 28 - 30, pp. 289 - 292 (2007).
- [12] W. Traupel. *Thermische Turbomaschinen. Klassiker der Technik, Band 1*. Springer-Verlag Berlin.
- [13] J. Luomi, C. Zwyssig, A. Looser, and J.W. Kolar. *Efficiency Optimization of a 100 W, 500 000 rpm Permanent-Magnet Machine Including Air Friction Losses*. in IEEE Industry Applications Conference 2007, New Orleans, USA, 2007.
- [14] C. Zwyssig, J.W. Kolar. *Design Considerations and Experimental Results of a 100 W, 500 000 rpm Electrical Generator*. Journal of Micromechanics and Microengineering, Issue 9, pp. 297 - 302, Sept. 2006.
- [15] C. Zwyssig, S.D. Round and J.W. Kolar. *Power Electronics Interface for a 100 W, 500 000 rpm Gas Turbine Portable Power Unit*. Applied Power Electronics Conference, Dallas, Texas, USA, March 19-23, pp. 283-289, 2006.